Numerical simulation of vertical buoyant wall jet discharged into a linearly stratified environment

Zhiyong Zhang[1];Yakun Guo[2]; Jian Zeng[3],Jinhai Zheng[4] and Xiuguang Wu[5]

Abstract: Results are presented from a numerical simulation to investigate the vertical buoyant wall jet discharged into a linearly stratified environment. A tracer transport model considering density variation is implemented. The standard k-ε model with the buoyancy effect is used to simulate the evolution of the buoyant jet in a stratified environment. Results show that the maximum jet velocity trend along vertical direction has two regions: acceleration region and deceleration region. In the deceleration region, jet velocity is reduced by the mixing taking place between jet fluid and ambient lighter fluid. Jet velocity is further decelerated by the upwards buoyant force when ambient fluid density is larger than jet fluid density. The normalized peak value of the cross sectional maximum jet velocity decreases with λ (the ratio between the characteristic momentum length and the buoyancy length). When λ<1, the dimensionless maximum penetration distance (normalized by the characteristic buoyancy length) does not vary much and has a value between 4.0 and 5.0, while it increases with increasing λ for $\lambda\geq$1. General good agreements between the simulations and measurements are obtained, indicating that the model can be successfully applied to investigate the mixing of buoyant jet with ambient linearly stratified fluid.

Keywords: Buoyant jet; stratification; maximum penetration distance; buoyancy number.

[1]Senior Engineer, Zhejiang Institute of Hydraulics and Estuary, Hangzhou, 310020, China.
[2] Professor, School of Engineering, University of Bradford, Bradford, BD7 1DP, UK. (Corresponding author). Email: y.guo16@bradford.ac.uk.
[3]Professor, Zhejiang Institute of Hydraulics and Estuary, Hangzhou, 310020, China.
[4]Professor, State Key Laboratory of Hydrology-Water Resources and Hydraulic Engineering, Hohai University, Nanjing 210098, China.
[5]Professor, Zhejiang Institute of Hydraulics and Estuary,Hangzhou,310020,China.

Introduction

Buoyant jet is a frequently encountered flow phenomenon in both natural and man-made environments. Typical examples are oil spillage from the underwater wells and sewage outfalls in the ocean, both have serious environmental impact. Due to its important environment impact and relevance to many scientific subjects, many studies have been conducted to investigate the spreading and dilution of buoyant jet discharging into a homogeneous environment using laboratory experiments (Turner 1966; Davidson et al. 2002; Marti et al. 2011) and numerical models (Kuang and Lee 2001; Huai and Fang 2006). These studies demonstrated many features of buoyant jet moving in a homogeneous environment. In many practical situations, however, the ambient fluid is stratified as shown in Fig.1. Such ambient stratification has significant effect on the motion of buoyant jet. Bloomfield and Kerr (1998) studied the turbulent fountains produced by injecting dense fluid upwards into linearly stratified ambient. They found that the momentum of injecting fluid was reduced by the opposing buoyancy force. Once the flow reached the maximum rising height, the fluid then flowed downwards and finally spread horizontally into ambient. Baines (2002) conducted laboratory experiments to investigate the two-dimensional vertical buoyant jet flowing downwards into strongly stratified fluid (see Fig.1b). The mixing of jet fluid with ambient fluid was estimated using a theoretical model developed. Wells and Nadarajah (2009) discussed the intrusion depth of density current in stratified water bodies based on laboratory experiments and oceanographic observations. They found that the intrusion depth was more sensitive to the ambient stratification than the buoyancy flux.

Comparing with large quantity laboratory experimental studies, relatively few numerical studies are reported to investigate the spreading and mixing of buoyant jet moving in a stratified

environment. Guo et al. (2014) performed numerical simulation to investigate the gravity current descending a mild slope into a linearly stratified ambient. However, the flow dynamics they studied is different from that of a buoyant wall jet vertically issuing into an ambient stratification. So far, references to the numerical modeling studies for buoyant jet discharging vertically into a stratified environment are still lacking and pose a challenge simulation task. In this study, a 2D model, FLUENT (ANSYS 12.0, 2009), with a user-defined tracer transport model, is employed to investigate the spreading and mixing of a vertical wall buoyant jet issuing into a linearly stratified environment. Such model considers the density variation induced by tracer concentrations. The model is validated using the experiments from Baines (2001, 2002). The validated model is then applied to simulate the evolution of a buoyant jet in a linearly stratified ambient for a range of flow parameters.

Mathematical Model

In this study, the standard k-ε model considering the buoyancy effect is used as the turbulence closure:

$$\frac{\partial}{\partial t}(\rho k)+\frac{\partial}{\partial x_i}(\rho u_i k)=\frac{\partial}{\partial x_i}[(\mu+\frac{\mu_t}{\sigma_k})\frac{\partial k}{\partial x_i}]+G_k+G_b-\rho\varepsilon \quad (1)$$

$$\frac{\partial}{\partial t}(\rho\varepsilon)+\frac{\partial}{\partial x_i}(\rho u_i \varepsilon)=\frac{\partial}{\partial x_i}[(\mu+\frac{\mu_t}{\sigma_\varepsilon})\frac{\partial \varepsilon}{\partial x_i}]+C_{1\varepsilon}\frac{\varepsilon}{k}(G_k+C_{3\varepsilon}G_b)-C_{2\varepsilon}\rho\frac{\varepsilon^2}{k} \quad (2)$$

where ρ= the density of mixture; t=time; k=turbulent kinetic energy; μ =the dynamic viscosity of fluid; u_i =the component of velocity in the x_i direction; ε=turbulent energy dissipation rate; μ_t=the dynamic turbulent (or eddy) viscosity; σ_k, σ_ε=the turbulent Prandtl number for k and ε, respectively, G_k=the generation of turbulence kinetic energy due to the mean velocity gradients; G_b=the generation of turbulence kinetic energy due to buoyancy, G_k and G_b can be determined as:

$$G_k = \rho \nu_t (\frac{\partial u_i}{\partial x_j} + \frac{\partial u_j}{\partial x_i}) \frac{\partial u_i}{\partial x_j} \quad (3)$$

$$G_b = -g_i \frac{\nu_t}{\sigma} \frac{\partial \rho}{\partial x_i} \quad (4)$$

where $\nu_t = C_\mu k^2/\varepsilon$=turbulent viscosity, σ is the turbulent Prandtl number.

The values of the coefficients in the turbulence model are (Rodi 1993): $C_{1\varepsilon}$=1.44, $C_{2\varepsilon}$=1.92, C_μ=0.09, σ_k=1.0, σ_ε=1.3, and σ=0.85. The coefficient $C_{3\varepsilon}$ is associated with the buoyancy term and can be evaluated as $C_{3\varepsilon}$=tanh|v/u| (Henkes et al.1991).

Generally speaking, one tracer can be defined to simulate the jet motion. However, the inflow fluid will mix with ambient fluid and it is difficult to capture the evolution of inflow fluid by using one tracer. Therefore, two tracers, α_1 and α_2, are defined in this study and the density at any position can be calculated as

$$\rho = \rho_w + \rho_s^1 C_1 + \rho_s^2 C_2 \quad (5)$$

where ρ_w (=1000 kg/m^3)=the density of fresh water; ρ_s^1 =the density of dry tracer α_1; ρ_s^2 =the density of dry tracer α_2; C_1=the concentration of tracer α_1; C_2=the concentration of tracer α_2. In this study, tracers α_1 and α_2 are defined as two different salts, but have the same density, namely $\rho_s^1 = \rho_s^2 = 2165\,\text{kg/m}^3$. The concentrations of each tracer should comply with the tracer transport equations. In this study, the relationship between density and tracer concentrations defined using User Defined Function (UDF), and User Defined Scalars (UDS) is used to solve the scalar transport equations in FLUENT.

Boundary and initial conditions

As there is little quantitative measurement for vertical buoyant jet issuing into a stratified ambient for model validation, cases of buoyant jet (or gravity current) flowing along a mild slope of θ=6° (see Baines (2001, 2002) for details) are used for model validation. Therefore, boundary and initial conditions are specified for both the flow moving along a slope (θ=6°) (see Fig.1a, not on scale) and vertically (θ=90°) (see Fig.1b) into a stratified ambient.

For θ=6°, at the inlet boundary, velocity is specified using the experimental data; namely the horizontal velocity u_0= Q_0/d_0(Q_0=the initial inflow discharge per unit length, d_0=inlet width);The turbulent kinetic energy, its dissipation rate and tracers concentrations are set as: $k_0 = (0.1u_0)^2$; ε_0=$10C_\mu^{3/4}k_0^{3/2}/(\kappa d_0)$(κ =the von Karman constant and taken as 0.41); C_1=0; $C_2 = C_2^0$ (C_2^0=tracer α_2 concentration at the inlet).The inflow density can be calculated as $\rho_{in} = \rho_w + \rho_s^2 C_2^0$. The top boundary is set as the symmetric boundary. The bottom and right hand side solid boundaries are set as no-slip wall boundary condition. For the parameters investigated in this study, the buoyant jet would not reach the bottom. As such the bottom solid boundary is ineffective. Standard wall function is employed to solve the velocity near the wall. The left boundary is set as outflow boundary condition in which a static pressure at the outlet boundary is realized (Guo et al. 2014).

For θ=90°, the inlet is on the right top and the velocity is set as u=0.0; v=v_0=Q_0/d_0. The turbulent kinetic energy, its dissipation rate and tracer concentrations are set as: $k_0 = (0.1v_0)^2$; ε_0=$10C_\mu^{3/4}k_0^{3/2}/(\kappa d_0)$; C_1=0; $C_2 = C_2^0$.The other boundary conditions are specified as the same as those in the case of θ=6°.

To establish the linearly stratified environment, the tracer in the tank at initial time satisfies the

following equations:

$$C_1(z) = (C_1^b - C_1^t)z / H + C_1^t \quad (6)$$

where C_1^b , C_1^t =the concentration of scalar α_1 at the bottom and the top of tank, respectively.

Numerical scheme

The computational domain is shown in Fig.1 with the tank length L=3m and the height H=0.23m for θ=6°,H=0.45m and 2.0m for θ=90°, respectively. The inlet width of the buoyant jet is d_0=0.01m. Body-fitted non-uniform meshes with arbitrarily spatially dependent size are used in the computational domain to improve the computational accuracy and save computational time (Guo et al. 2012). This arrangement also allows for locally refining the concerned regions (e.g. near inlet region) with small meshes and has the advantage of flexibly assigning meshes in the computational domain (Guo et al. 2008). Boundary layer mesh is used to make the standard wall function run well and the dimensionless nearest grid size on the right wall is set between 30.0 and 500.0.The pressure and velocity coupling are solved by using the SIMPLE algorithm. The time step is $\triangle t$=0.005s. The results analyzed and presented in this study are taken from the simulation when the quasi-steady state is reached.

Result and discussion

The laboratory experiments of Mitsudera and Baines (1992) and Baines (2001, 2002) are used to validate the numerical model. Wright and Wallace (1979) showed that the motion of the buoyant jet in stratified environment is related to the kinematic source momentum flux at the inlet M_0=v_0Q_0, the source buoyancy flux at the inlet B_0= $g_0^{'}Q_0$ and the ambient buoyancy frequency N=[(g/ρ_1)(ρ_2-ρ_1)/H]$^{1/2}$ where $g_0^{'}$=the reduced gravity acceleration and $g_0^{'} = g(\rho_{in} - \rho_1)/\rho_1$. For

convenience of the analysis and to compare with the experimental measurements, an along (s) and normal to the slope (r) coordinate system s-r is established (see Fig.1a. Note that the simulation is performed in x-z coordinate system). In this coordinate system, u_s refers to the downslope component of velocity. For the cases of θ=90° (Fig.1b), the s-r coordinate system coincides with the x-z coordinate system.

To distinguish the buoyancy-dominated jet and momentum dominated jet, Wright and Wallace (1979) defined a parameter λ:

$$\lambda = l_M / l_b = \frac{Q_0 N}{d_0 g_0'} \tag{7}$$

where $l_M=(M_0/B_0^{2/3})$=the characteristic momentum length scale which shows the importance of the initial momentum, $l_b=(B_0^{1/3}/N)$ = the characteristic buoyancy length scale which shows the importance of the buoyant force. From the definition, if λ<1, the buoyant force is more significant than the momentum and the flow is buoyancy dominated. For λ>1, the momentum is more important than the buoyancy. For extremely situation of $\lambda\to\infty$ and $\rho_{in}\neq\rho_1$, the flow behaves as a pure momentum jet.

Numerical simulations have been performed to reproduce 10 experimental cases for comparison purpose as well as another 12 cases to expand the range of λ and Reynolds number (R). These additional 12 cases are simulated to examine the effect of R on the evolution of jet as well as to investigate the motion characteristics of both the buoyancy dominated jet (relatively small λ) and the momentum dominated jet (relatively large λ). The parameters of the cases simulated are listed in Table 1 in which Case 1 to Case 10 are experiments (Baines 2001, 2002). Only Case 10 of $\theta=6^o$ has

156 the detailed measurements and is used to validate the model.

157

158 ***Validation of the numerical model***

159 To examine the simulation accuracy, both 2D and 3D runs have been performed for Case 10 in
160 which the 3D simulation channel width is taken as the same as in the experiments (Baines 2001).
161 Fig.2 shows the comparison of the 2D and 3D numerical simulation and laboratory experimental
162 measurements of the velocity profiles at s=0.9m for Case 10. The 3D velocity profile is extracted
163 from the central plane of the domain. Fig.2 demonstrates that 3D simulation has no significant
164 improvement over that by 2D model while its computational time is almost 4 times of that in 2D
165 simulation. Therefore, the following results are based on 2D numerical simulations. Fig.3 is the plot
166 of the simulated and measured density distribution at s=0.7m for Case 10. It is seen from Fig. 2 and
167 3 that a good agreement between the simulation and measurement is obtained, indicating that the
168 numerical model has sufficient accuracy to calculate the velocity and density field of the buoyant jet
169 moving in a linearly stratified environment.

170

171 ***Grid independence***

172 Grid independence has been conducted to assure the reliability of numerical simulation result. Table
173 2 lists the normalized peak jet velocity v_m/v_0 and the maximum penetration distance z_m/l_b for Case 2
174 with three grid sizes. The jet maximum penetration distance is defined as the vertical distance
175 measured from the inlet to the position where the jet downwards velocity is reduced to zero. In
176 practice, the position where the downwards velocity near the wall is less than $0.01v_0$ is defined as
177 the location where the maximum penetration distance reaches. Three grid numbers simulated are
178 213044,150384 and 103680 with the minimum space along the x direction being 0.0002m, 0.0005m

and 0.0008m respectively. Table 2 shows that both the normalized peak jet velocities and the maximum penetration distance obtained from three meshes are very close with the maximum relative error being smaller than 0.6%. Considering the simulation accuracy and the computational efficiency, the final meshes used in this study is taken as 103680.

Velocity profile

As described in previous work (Baines 2002), when the buoyant jet enters into the stratified environment, mixing and entrainment between flow fluid and ambient lighter fluid occurs, which dilutes the jet fluid and makes the flow grow. This process continues until the flow momentum and buoyancy is balanced or the driving force is less than the wall friction and ambient stratification at a certain depth. Jet flow then springs upwards and spreads horizontally into environment.

Fig.4 is the vertical velocity distributions at the cross sections of z/d_0=5 (Fig4.a) and 20 (Fig4.b) for five simulation conditions. At the section close to the inlet (z/d_0=5), the top hat velocity profiles (Guo 2014) are found for larger R (R>1000). This may imply that the flow is in the zone of potential core region. The flow thickness increases with the inflow R as stronger mixing and entrainment between the inflow and ambient fluid occurs for higher R. The maximum cross sectional jet velocity is slightly larger than the inlet velocity due to the initial downward buoyant force. For lower R flow (R=269.7), the flow velocity increases sharply from zero on the wall (where no-slip condition is applied) to the maximum at about x=0.2d_0, and then decreases to nearly zero at x=0.8d_0, demonstrating a typical wall jet self-similarity velocity profile. This velocity profile is different from those of higher R flow. This may be ascribed to the fact that the initial flow downward buoyant force for R=269.7 is relatively large due to weak mixing and entrainment taking

place between the flow fluid and the ambient fluid, resulting in a narrow and quickly accelerated jet flow. At $z=20d_0$, flow is fully developed and has the typical wall jet flow velocity profile for larger R. It is seen that the maximum cross sectional jet velocities are slightly larger than the values at $z=5d_0$ due to the continuous acceleration driven by downward buoyant force. For the case of $R=269.7$, as jet continues to descend, mixing and entrainment between flow fluid and ambient lighter fluid is enhanced, thereby reducing the downward driving buoyancy force. As such, jet is decelerated. Fig. 4b also demonstrates that there is a negative velocity at $x/d_0>3.0$ for $R=269.7$. Analysis of the simulation data for $R=269.7$ shows that the jet flow has almost reached its maximum penetration distance at $z=20d_0$ (see Fig. 5) where the jet fluid away from the wall begins moving upwards, thereby generating the negative (upwards) velocity between $x/d_0=3.0$ and $x/d_0=5.0$.

The cross sectional maximum jet velocity

Fig.5 is the normalized local cross sectional maximum jet velocity along vertical distance from the inlet. For the purpose of clarification, only simulations for six cases are plotted. Fig.5 shows that the normalized cross sectional maximum flow velocity initially increases with the distance and reaches a peak value whose position is further downward with the increase of inflow R. For small R (laminar jet), initial mixing and entrainment is weak, resulting in larger normalised jet peak velocity. While for large R flow (turbulent jet), stronger mixing and entrainment occurs once the jet enters into ambient fluid, which significantly dilutes jet fluid and results in a relatively small jet peak velocity.

As analysed above, the cross sectional maximum jet velocity v_{sm} reaches a peak value v_m at a certain vertical distance. This peak velocity v_m is the maximum velocity that a buoyant jet can reach for a given flow and ambient conditions. This maximum jet velocity is therefore related to the initial jet momentum, the ambient stratification, the initial reduced gravity of jet fluid and the fluid viscosity and could be expressed as following:

$$v_m = f(v_0, d_0, \rho_1, N, (\rho_{in} - \rho_1)g, \mu) \tag{8}$$

Selecting v_0, d_0 and ρ_1 as basic dimensions and applying the π-theorem yields

$$\frac{v_m}{v_0} = f(\frac{Nd_0}{v_0}, \frac{(\rho_{in} - \rho_1)gd_0}{v_0^2\rho_1}, \frac{\mu}{v_0 d_0 \rho_1}) \tag{9}$$

where $\mu/(v_0 d_0 \rho_1)$ is $1/R$.

As discussed above, parameter λ could be used to distinguish if jet is dominated by initial momentum or buoyancy and analyzing equation (9) reveals that the combination of the first and second items on the right hand side of (9) is λ, i.e. $\lambda = (\frac{Nd_0}{v_0}) / [\frac{(\rho_{in} - \rho_1)gd_0}{v_0^2\rho_1}]$. As such, it is reasonable to analyze the relationship of the dimensionless maximum jet velocity with λ and R.

Another important parameter of the motion of the buoyant jet is the maximum penetration distance z_m, which can be expressed as (Wright and Wallace 1979):

$$\frac{z_m}{l_b} = f(\frac{l_M}{l_b}) = f(\lambda) \tag{10}$$

Fig.6 is the simulated normalised maximum velocity versus λ for all cases investigated. It is seen from Fig.6 that for λ<1.0, the buoyant force plays more significant role, implying that the mixing

and entrainment between jet fluid and ambient fluid is weak, leading to less dilution of jet fluid. As such, the normalised maximum velocity increases with the decrease of λ. While for $\lambda \geqslant 1$, the jet momentum becomes more dominant. Strong velocity shear is formed at the interface of the jet fluid and the ambient fluid as jet descends. This strong shear velocity generates significant mixing and greatly entrains ambient lighter fluid into jet, resulting in great dilution of the jet fluid. Consequently, the normalised maximum velocity v_m is small and close to the jet velocity (v_0) at the inlet.

To investigate the effect of R on the maximum jet velocity, simulations are divided into four groups in which each group has similar λ value (e.g. $\lambda \approx 0.2$ for case 5 and case 14; $\lambda \approx 0.4$ for case 7 and case 15; $\lambda \approx 1.0$ for case 8 and case 12 and $\lambda \approx 2.6$ for case 19 and case 20). Fig.7 plots the variation of the normalized maximum velocity versus different R. It is seen that for the same λ, the variation of inflow R has insignificant effect on the normalized maximum jet velocity, particularly, for large inflow R jet. This is contrary to the significant impact of λ on the maximum velocity, implying that the maximum jet velocity mainly depends on λ rather than R.

The maximum penetration distance

Wright and Wallace (1979) analyzed the free buoyant jet moving in a linearly stratified environment and found that when $\lambda<1$ the dimensionless maximum penetration distance z_m/l_b was nearly a constant of 3.6, and z_m/l_b increased with λ when $\lambda \geq 1$. To compare with the free buoyant jet, Fig.8 plots the variation of the simulated and measured (Baines 2002) dimensionless maximum penetration distance of the buoyant wall jet with λ and R regions. It is seen that in general, the inflow R has insignificant effect on the maximum penetration distance. Fig. 8 also shows that when $\lambda<1$, the dimensionless maximum penetration distance z_m/l_b has no significant change with the

variation of λ. The dimensionless maximum penetration distance has a value between 4.0 and 5.0, which is larger than the value of the free buoyant jet. This can be ascribed to the fact that the mixing and entrainment takes place at two free boundaries for free jet while for wall jet, these events only occur at one free boundary. Therefore, mixing and entrainment for free jet is higher than that for wall jet for otherwise identical conditions. For$\lambda \geqslant 1$, the maximum penetration distance significantly increases with the increase of λ. Fig.8 also shows that the simulated maximum penetration distance favorably compares with the measurements.

Conclusions

A two-dimensional *k-ε* mathematical model and tracer transport model considering density changes are established within the framework of FLUENT. The model is applied to compute the buoyant wall jet vertically discharged into the linearly stratified environment. The developed model is firstly validated using the laboratory measurements for gravity current descending a mild slope into stratified ambient. The validated model is then employed to simulate the flow evolution of the vertical buoyant wall jet for a wide range of λ and R. The velocity field, density distributions and the maximum penetration distance are simulated and compared with the available experimental measurements. Simulated results demonstrate that the ambient stratification, reduced gravity acceleration of jet fluid and the initial jet momentum have significant effects on the motion and spreading of the buoyant wall jet. As the flow descends, interfacial velocity shear generates mixing and entrainment at the free boundary/interface between the jet fluid and the ambient fluid, leading to the dilution of the jet fluid. As jet continues to descend, the downwards buoyant force further decreases and eventually becomes upward force, thereby decelerating jet motion. For buoyancy dominant wall jet (λ<1), the peak value of the cross sectional maximum jet velocity increases with the decrease of λ, while for momentum dominant wall jet, the normalized peak velocity remains

roughly as a constant of 1.0.

For buoyant dominant wall jet (λ<1), the normalized maximum penetration distance has a value about 4.0-5.0, which is larger than that of free buoyant jet. This is mainly ascribed to the fact that the free jet has two free boundaries and generates greater mixing and entrainment than wall bounded jet does.

The study has potential engineering and environmental application for predicting the spreading and dispersion of negative effluent discharged into receiving stratified water bodies (e.g. heavy wastewater outfall, submerged outfall from desalination plants (Gildeh et al. 2014)).

Acknowledgements: The research reported in this paper is financially supported by UK Engineering and Physical Sciences Research Council (EPSRC: EP/G066264/1), National Natural Science Foundation of China (51609214,41376099,51609213), National Natural Science Foundation for Distinguished Young Scholars of China (Grant No.51425901),Public Project of Zhejiang Province (2016C33095) and Key Project of Zhejiang Science and Technology(2015C03003). The comments and suggestions made by the Chief Editor, the Associate Editor and Reviewers have significantly improved the quality of the manuscript

Notations

The following symbols are used in this Technical Note:

B_0=buoyancy flux per unit length at inlet

315 C_1 ,C_2=tracer concentration ofα_1,α_2 respectively

316 C_1^b, C_1^t=tracer α_1 concentration at the bottom and top of tank respectively

317 C_2^0=tracer concentration of α_2 at inlet

318 d_0=initial width of jet

319 G_k,G_b=generations of turbulence kinetic energy due to the mean velocity gradients and buoyancy

320 respectively

321 g= gravity acceleration

322 $g_0^{'}$=the reduced gravity acceleration

323 H=tank height

324 k= turbulent kinetic energy

325 L= tank length

326 l_M=characteristic momentum length

327 l_b=characteristic buoyancy length

328 M_0=moment flux per unit length at inlet

329 N= ambient buoyancy frequency

330 Q_0=initial volumetric flux per unit slot width

331 R=Reynolds number

332 r= coordinate normal to the slope

333 s=coordinate along the slope measured from the top of slope

334 t=time

335 $\triangle t$=time step

336 u= velocity component along the x direction

337 u_s= velocity component along the slope

338 v=velocity component along the z direction

339 v_0=velocity along the z direction at the inlet

340 v_{sm}=the maximum jet velocity at different x- cross section

341 v_m=the peak value of v_{sm}

342 x=horizontal coordinate

343 z=vertical coordinate

344 z_m=maximum penetration distance

345 ε=turbulent dissipation rate

346 κ=Von Karman constant

347 $\lambda=l_M/l_b$ =the ratio between characteristic momentum and buoyancy length

348 μ,μ_t=dynamic viscosity and dynamic turbulent viscosity respectively

349 θ=slope angle

350 ρ= mixture density

351 ρ_w= pure water density

352 ρ_1= density at the top

353 ρ_2=density at the bottom

354 ρ_{in} = inflow fluid density

355 ρ_s^1, ρ_s^2 =dry tracerα_1,α_2density respectively

356 σ=turbulent Prandtl number

357 $\sigma_k,\sigma_\varepsilon$=turbulent Prandtl number for k, ε respectively

358

359 **References**

360 ANSYS FLUENT (2009). “Theory Guide and User’s Guide, version 12.0.” ANSYS, Inc.

Southpointe, Canonsburg, U.S.

Baines, P.G. (2001). "Mixing in flows down gentle slopes into stratified environments." *J. Fluid Mech.*443, 237-270.

Baines, P.G. (2002). "Two-dimensional plumes in stratified environments." *J. Fluid Mech.*471, 315-337.

Bloomfield, L.J., and Kerr, R.C. (1998). "Turbulent fountains in a stratified fluid." *J. Fluid Mech.*,358, 335-356.

Davidson, M.J., Gaskin, S., and Wood, I.R., (2002). "A study of a buoyant axisymmetric jet in a small co-flow." *J. Hydraul. Res.*, 40(4),477-489.

Gildeh1, H.K., Mohammadian, A., Nistor, I. and Qiblawey, H. (2014). "Numerical modeling of turbulent buoyant wall jets in stationary ambient water." *J. Hydraul. Eng.*, 140(6), 10.1061/(ASCE)HY.1943-7900.0000871, 04014012.

Guo, Y.K. (2014). "Numerical simulation of the spreading of aerated and nonaerated turbulent water jet in a tank with finite water depth." *J. Hydraul. Eng.*, 140(8). 10.1061/(ASCE)HY.1943-7900.0000903.

Guo, Y.K., Zhang, L.X., Shen, Y.M. and Zhang, J.S., 2008. Modelling study of free overfall in a rectangle channel with strip roughness, *J. Hydraul. Eng.*, 134(5), 664-668.

Guo, Y.K., Zhang, Z.Y. and Shi, B. (2014). "Numerical simulation of gravity current descending a slope into a linearly stratified environment." *J. Hydraul. Eng.*, 140(12) 10.1061/(ASCE)HY.1943-7900.0000936

Guo, Y.K., Wu, X.G., Pan, C.H. and Zhang, J.S. (2012). "Numerical simulation of the tidal flow and suspended sediment transport in the Qiantang Estuary." *J. Waterway, Port, Coastal and*

383 *Ocean Eng.*, 138(3), 192-203.

384 Henkes, R. A., W. M. Flugt, F. F., and Hoogendoorn, C. J., (1991). "Natural convection flow in a
385 square cavity calculated with low-Reynolds number turbulence models." *Int. J. Heat Mass*
386 *Transfer*, 34, 1543–1557.

387 Huai, W.X., and Fang, S.G., (2006). "Numerical Simulation of Obstructed Round Buoyant Jets in a
388 Static Uniform Ambient." *J. Hydraul. Eng.*, 132(4), 428-431.

389 Kuang, C.P., and Lee, J.H.W., (2001). "Effect of downstream control on stability and mixing of a
390 vertical plane buoyant jet in confined depth." *J.Hydraul.Res.*,39(4),375-391

391 Marti, C.L., Antenucci, J.P., Luketina, D., Okely,P., and Imberger, J., (2011). " Near-Field Dilution
392 Characteristics of a Negatively Buoyant Hypersaline Jet Generated by a Desalination Plant." *J.*
393 *Hydraul. Eng.*, 137(1), 57–65.

394 Mitsudera, H. and Baines, P. G. (1992). Downslope gravity currents in a continuously stratified
395 environment: a model of the Bass Strait outflow. *Proc., 11th Australasian Fluid Mechanics*
396 *Conference*, Hobart, Australia, 1017–1020.

397 Rodi, W. (1993). *Turbulence models and their application in hydraulics: a state-of-the-art review*.
398 IAHR Monograph, 3rd edition, A.A. Balkema.

399 Turner, J.S., (1966)."Jets and plumes with negative or reversing buoyancy." *J. Fluid Mech.*,26(4),
400 779-792

401 Wells, M., and Nadarajah, P., (2009)."The Intrusion Depth of Density Currents Flowing into
402 Stratified Water Bodies." *J. Phys. Oceanogr.*,39, 1935-1947.

403 Wright, S. J., and Wallace, R.B., (1979) "Two-Dimensional Buoyant Jets in Stratified Fluid." *J.*
404 *Hydraul. Eng.*, 105(11), 1393–1406.

405 Table 1 Parameters of computational cases

Case No.	H (m)	λ	Re	Q_0 (m^2/s)	$g_0^{'}$ (m/s^2)	N (1/s)	θ
1		0.07	269.7	0.0002697	0.4087	1.03	90
2		0.08	269.7	0.0002697	0.3400	0.98	90
3		0.11	269.7	0.0002697	0.1900	0.74	90
4		0.16	409.1	0.0004091	0.1747	0.69	90
5	0.45	0.24	409.1	0.0004091	0.0791	0.46	90
6		0.33	1036	0.001036	0.2800	0.90	90
7		0.43	688.0	0.000688	0.1259	0.79	90
8		1.01	1385.4	0.001385	0.1166	0.85	90
9		1.35	1385.4	0.001385	0.0662	0.65	90
10	0.23	0.233	290.0	0.000290	0.1494	1.20	6
11		0.50	1000	0.001	0.0981	0.49	90
12		1.00	2000	0.002	0.0981	0.49	90
13		2.02	4000	0.004	0.0981	0.49	90
14		0.20	1000	0.001	0.2800	0.49	90
15		0.40	2000	0.002	0.2800	0.49	90
16	2.0	0.81	4000	0.004	0.2800	0.49	90
17		0.64	1000	0.001	0.0981	0.62	90
18		1.28	2000	0.002	0.0981	0.62	90
19		2.55	4000	0.004	0.0981	0.62	90
20		2.55	2000	0.002	0.0490	0.62	90
21		5.11	4000	0.004	0.0490	0.62	90
22		7.66	6000	0.006	0.0490	0.62	90

406
407

408 Table 2 variation of peak jet velocity and maximum penetration distance with mesh densities (case 2)

409

Mesh grids number	Minimum space(m)	v_m/v_0	z_m/l_b
103680	0.0008	5.149	4.548
150384	0.0005	5.152	4.571
213044	0.0002	5.153	4.575

410
411
412
413
414

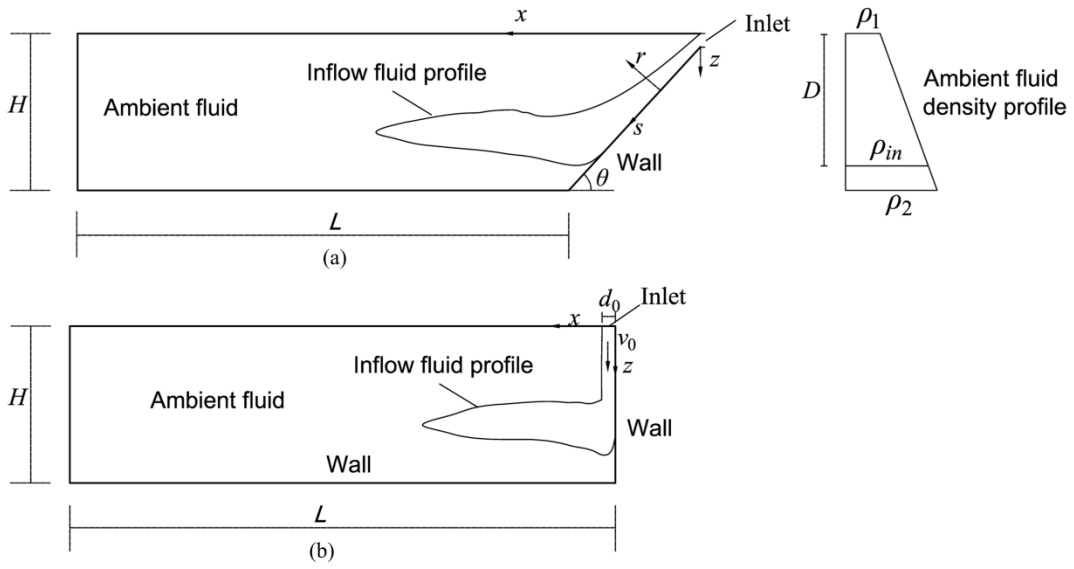
x
Inlet
r
z
Inflow fluid profile
H
Ambient fluid
s
Wall
θ
L
(a)
ρ1
D
Ambient fluid
density profile
ρin
ρ2
d0
Inlet
x
v0
z
Inflow fluid profile
H
Ambient fluid
Wall
Wall
L
(b)

Figure 1

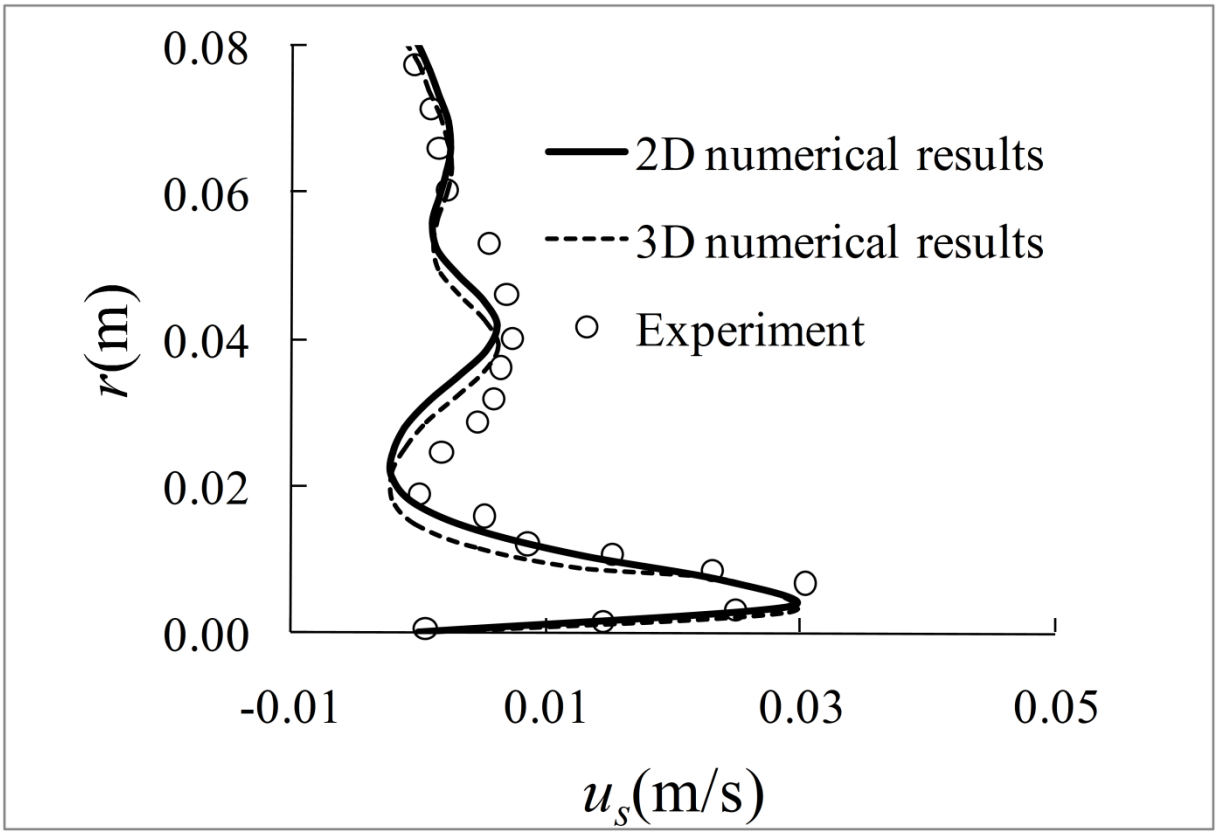

428

429 Figure 2

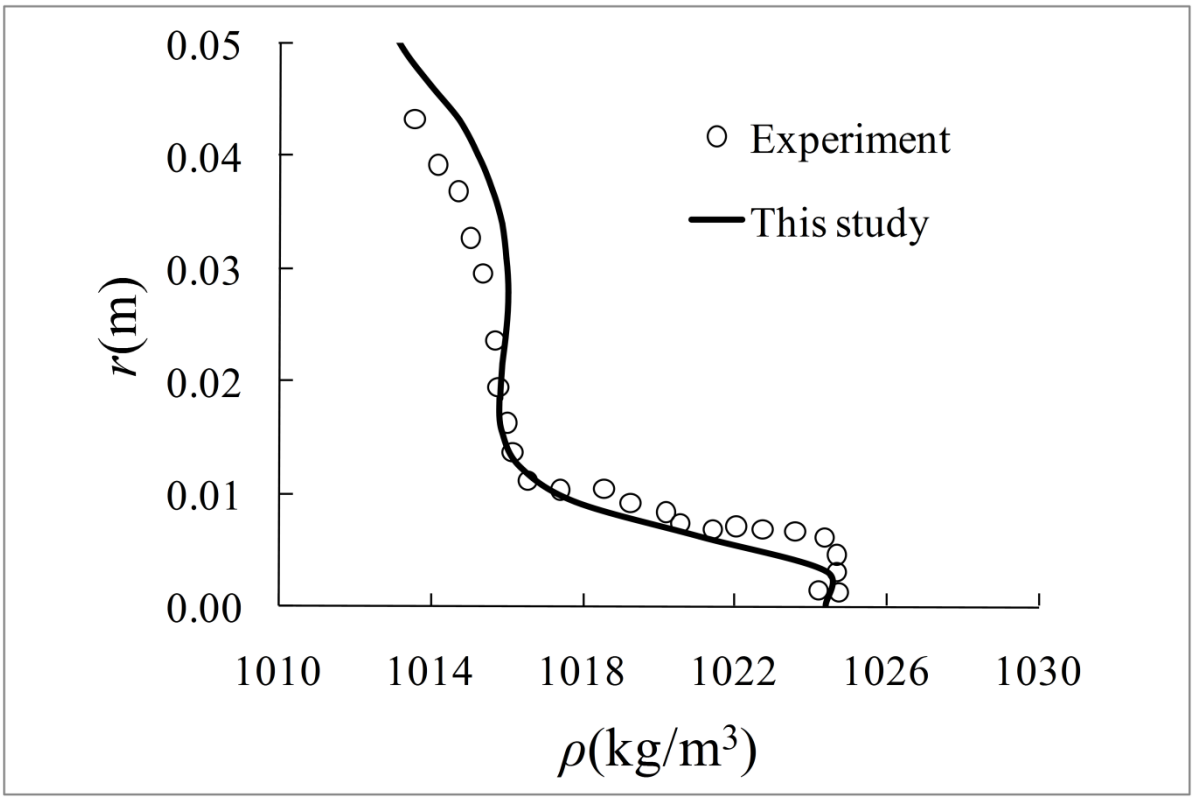

430

431 Figure 3

432

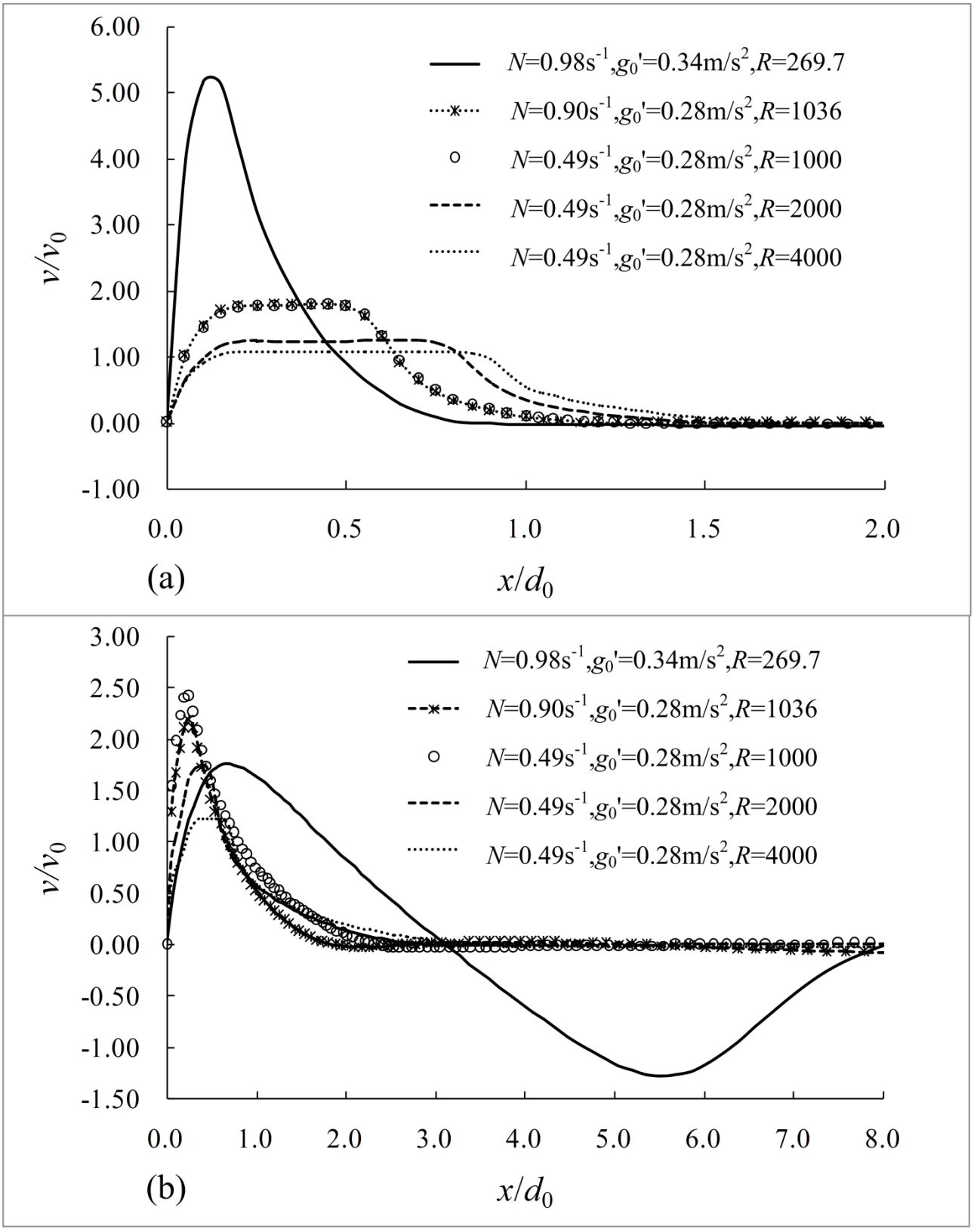
6.00
5.00
4.00
3.00
2.00
1.00
0.00
-1.00
v/v0
N=0.98s-1,g0'=0.34m/s2,R=269.7
N=0.90s-1,g0'=0.28m/s2,R=1036
N=0.49s-1,g0'=0.28m/s2,R=1000
N=0.49s-1,g0'=0.28m/s2,R=2000
N=0.49s-1,g0'=0.28m/s2,R=4000
0.0
0.5
1.0
1.5
2.0
(a)
x/d0
3.00
2.50
2.00
1.50
1.00
0.50
0.00
-0.50
-1.00
-1.50
v/v0
N=0.98s-1,g0'=0.34m/s2,R=269.7
N=0.90s-1,g0'=0.28m/s2,R=1036
N=0.49s-1,g0'=0.28m/s2,R=1000
N=0.49s-1,g0'=0.28m/s2,R=2000
N=0.49s-1,g0'=0.28m/s2,R=4000
0.0
1.0
2.0
3.0
4.0
5.0
6.0
7.0
8.0
(b)
x/d0

Figure 4

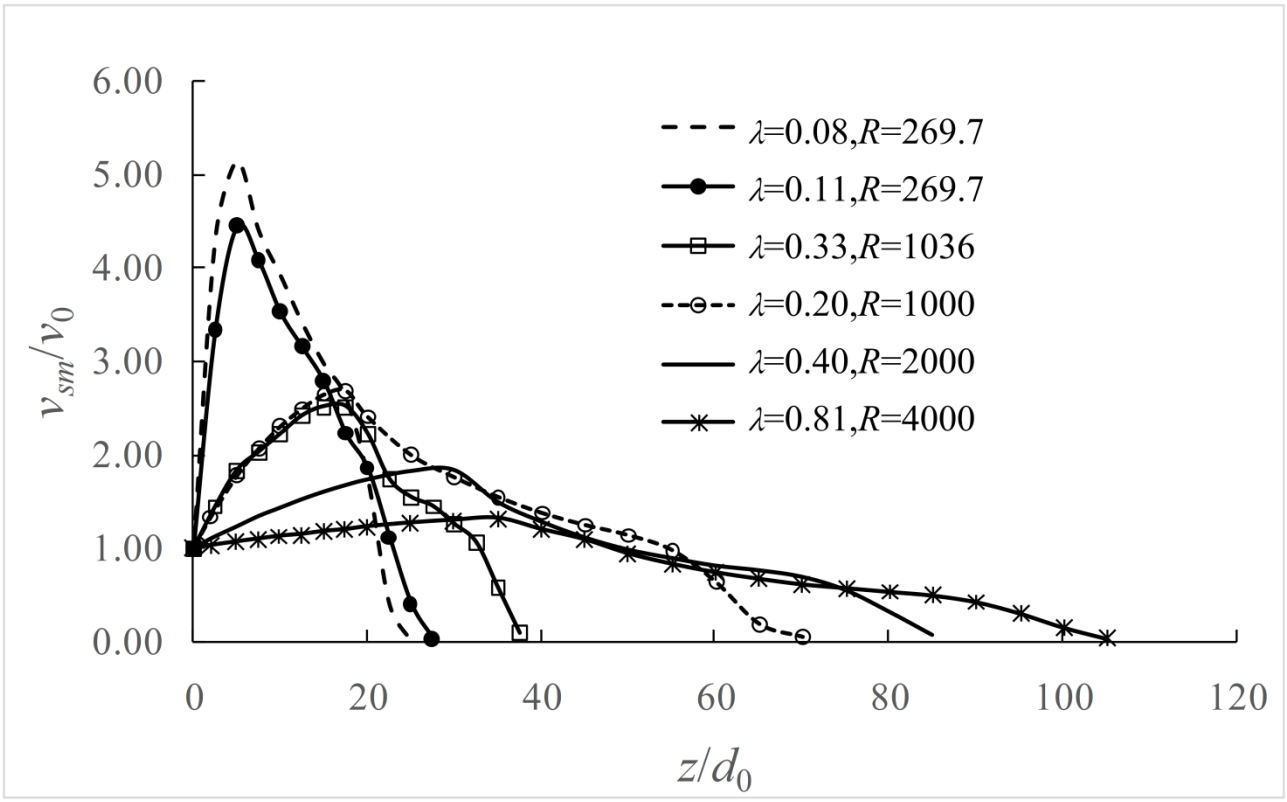

437

438 Figure 5

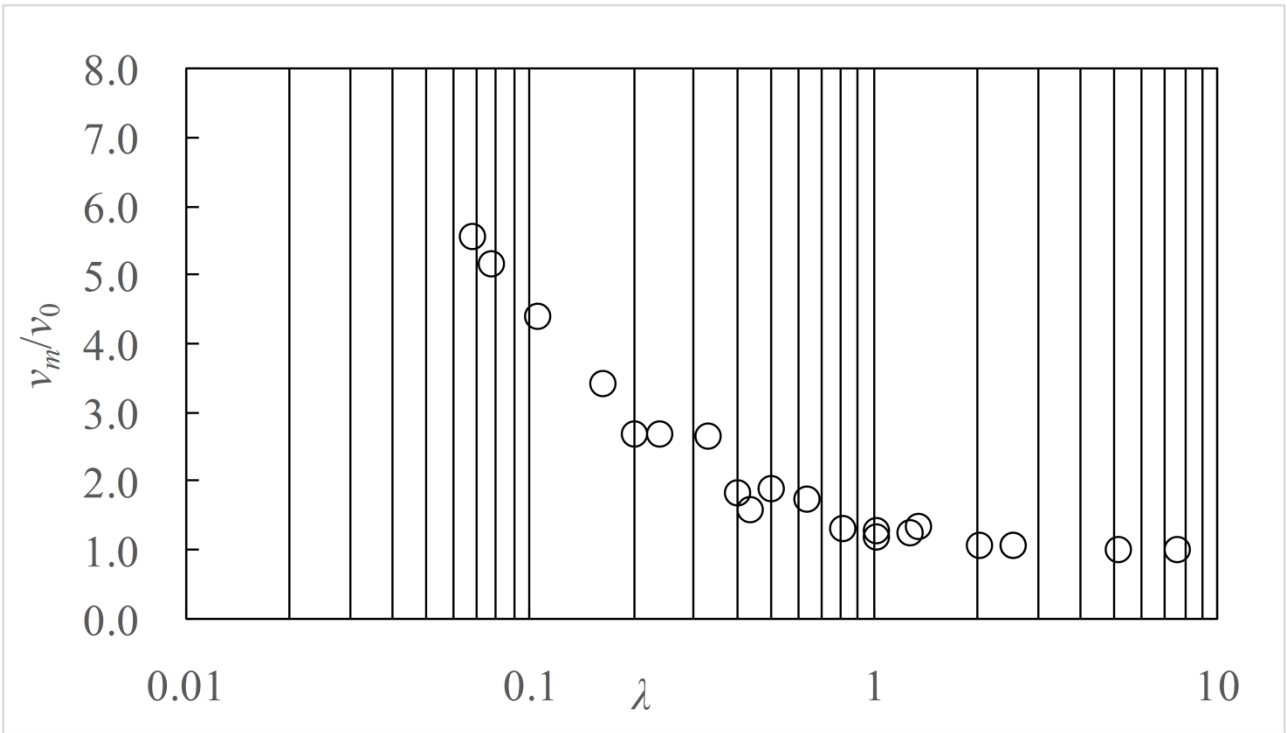

439

440 Figure 6

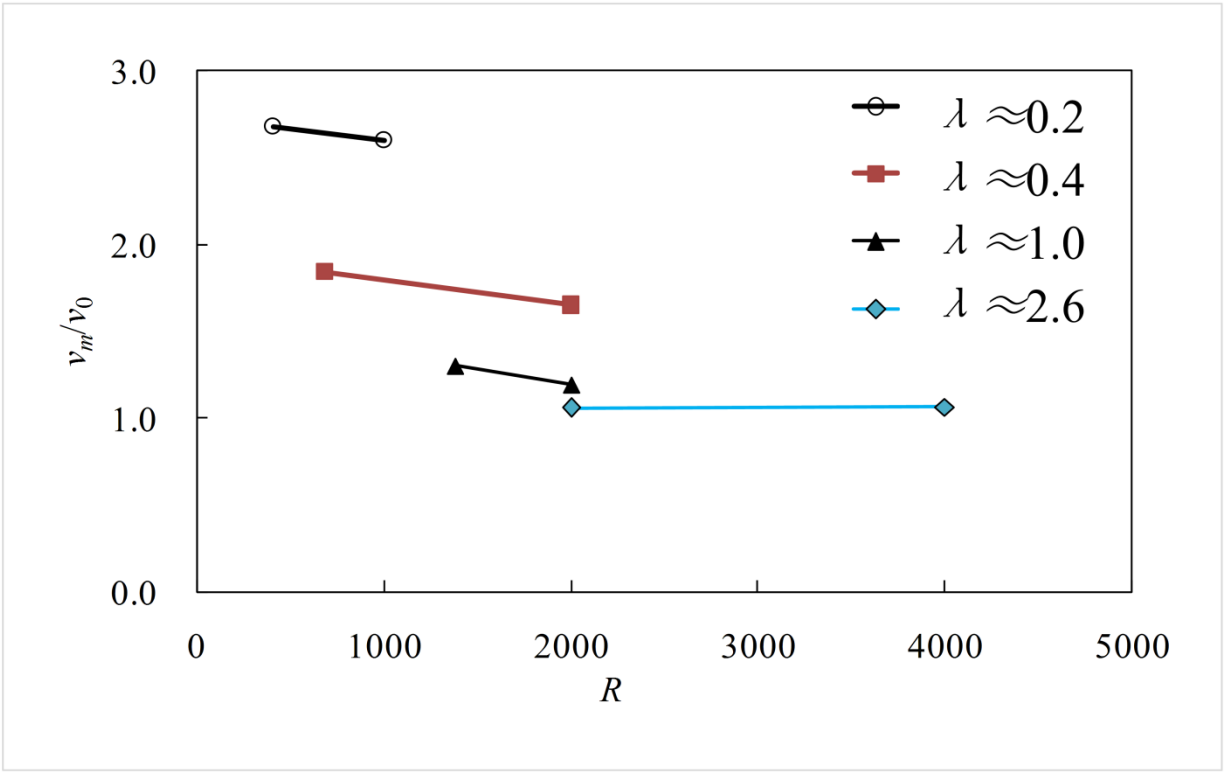

441

442 Figure 7

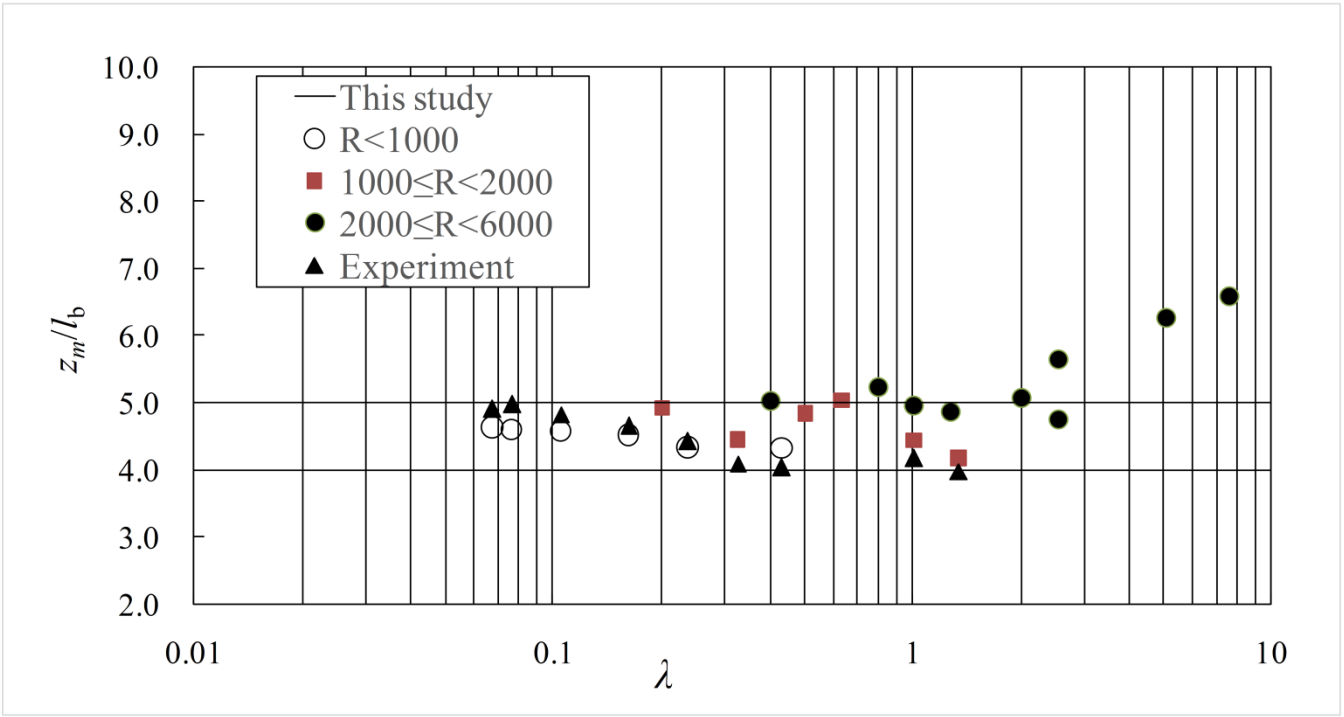

443

444 Figure 8

445

446 Fig.1 Schematic diagram of the model and coordinate system: (a) slope (b) vertical condition.

447 Fig.2 Comparison of the simulated 2D and 3D velocity profiles at s=0.9 m for Case 10.
448 Experimental measurements by Baines (2001) are plotted for validation.

449 Fig.3 Comparison of the simulated (2D and 3D) and measured (data from Mitsudera and Baines
450 1992) density profiles at s=0.7 m for Case 10.

451 Fig.4 Simulated velocity profiles at two vertical positions: (a) z/d_0=5.0 (b)z/d_0=20.0

452 Fig.5 Simulated local maximum velocity along the vertical distance from the inlet. Velocity is
453 normalized by using the velocity at the inlet

454 Fig.6 Variation of the normalized peak jet velocity with λ

455 Fig.7 Variation of the normalized peak jet velocity with R

456 Fig.8. Variation of the normalized maximum penetration distance z_m/l_b with λ

457

458